Journal of Porous Media 13(12), 1039–1058 (2010)

THE INSTABILITY OF A DEVELOPING THERMAL FRONT IN A POROUS MEDIUM. III SUBHARMONIC INSTABILITIES

Asma Selim & D. Andrew S. Rees*

Department of Mechanical Engineering, University of Bath, Claverton Down, Bath BA2 7AY, United Kingdom

*Address all correspondence to D. Andrew S. Rees E-mail: ensdasr@bath.ac.uk

Original Manuscript Submitted: 12/29/2008; Final Draft Received: 6/12/2009

In this paper we study the instability of the developing thermal boundary layer that is induced by suddenly raising the temperature of the lower horizontal boundary of a uniformly cold semi-infinite region of saturated porous medium. The basic state consists of no flow, but the evolving temperature field may be described by a similarity solution involving the complementary error function. In very recent papers, Selim and Rees (2007a) (Part I) have sought to determine when this evolving thermal boundary layer becomes unstable and then Selim and Rees (2007b) (Part II) followed the subsequent evolution of horizontally periodic disturbances well into the nonlinear regime. In this paper we investigate the secondary instability of the nonlinear cells by introducing subharmonic disturbances into the evolving flow. We consider three different types of subharmonic disturbance, namely, the 2:1, 3:2, and 4:3 types. Cellular disturbances are seeded into the evolving basic state, the primary mode having an amplitude that is greater than that of the subharmonic. In general, we find that the subharmonic decays at first, while the primary mode grows, but at a time that is dependent on the relative initial amplitudes, the subharmonic experiences an extremely rapid growth and quickly establishes itself as the dominant flow pattern. A fairly detailed account of the 2:1 case is given, including an indication of how the time of transition between the primary and the subharmonic varies with wave number and initial amplitudes. The other two types of subharmonic disturbance yield a richer variety of behaviors; therefore, we present some typical cases to indicate some of the ways in which the primary mode may be destabilized.

KEY WORDS: *boundary layer, secondary instability, sub-harmonic disturbances*

1. INTRODUCTION

The study of convection generated by a heated horizontal surface underlying a fluid-saturated porous medium has attracted much interest in recent years due to its application to the sudden heating of porous rocks from below such as might occur in volcanically active regions. Recently, convection induced by the sequestration of CO_2 in saturated porous rocks during oil recovery has received attention (Riaz et al., 2006). Indeed, such convection could easily occur during the long-term underground storage of CO_2 gas, as described by Xu et al. (2004), Socolow (2005), and Ennis-King and Paterson (2005), when surface pollutants are present, or indeed when surface evaporation increases the brine density near the surface of a saline lake (Wooding et al. 1997). In all of these cases the presence of thermal or solutal instability will cause an increased mixing, which is generally undesirable. In this paper we shall analyze situations caused by sudden heating as the exemplar of the two different cases, although they are essentially identical when the Boussinesq approximation applies.

When a semi-infinite cold domain has the temperature of its lower impermeable surface raised suddenly, the temperature field evolves according to the standard complementary error function conduction solution, as given by

1091–028X/10/$35.00

NOMENCLATURE

a	related to disturbance amplitude
A	amplitude of disturbance
g	gravity
k	wavenumber of disturbance
K	permeability
L	natural length scale
N	number of modes used
p	pressure
q	heat transfer
q_n	heat transfer for mode n
Ra	Darcy–Rayleigh number
t	time
T	dimensional temperature
u	horizontal velocity
v	vertical velocity
x	horizontal coordinate
y	vertical coordinate

Greek characters

α	thermal diffusivity
β	expansion coefficient
η	similarity variable
θ	nondimensional temperature
μ	dynamic viscosity
ρ	density
τ	scaled time
ψ	streamfunction

Superscripts and subscripts

c	neutral/critical conditions
i	initiation time
s	subharmonic transition
w	wall
∞	ambient

Carslaw and Jaeger (1986). This situation is potentially unstable since relatively heavy fluid lies over relatively light fluid. A Rayleigh number may be defined using a length scale that is based upon the thickness of the evolving hot region. This value increases as time progresses, and therefore a critical time for the onset of convection should be expected. Rees et al. (2008) discuss the many ways in which this criterion for the onset of convection may be obtained. Various methods have been proposed such as quasistatic theory (i.e., a frozen-time theory) and a local Rayleigh number analysis, which are approximate, but which give a rough idea of the time of onset and the expected critical wave number. Energy analyses and amplitude theory (in the sense of solving the time-dependent disturbance equations) yield results that should be expected to tally with experimental results. However, these comparisons and the discussions surrounding them are lengthy; therefore, the reader is referred to Rees et al. (2008), and the references cited therein for further information.

The present paper is an extension of work by Selim and Rees (2007a, 2007b), hereafter referred to as Parts I and II. The former of these papers did not rely upon an approximate theory to give a critical time for the onset of convection. Instead, the full linearized disturbance equations, which are parabolic in time, were solved numerically in order to assess when disturbance ceases to decay and begins to grow, thereby determining a critical time. After a large number of different disturbance wavelengths was considered, a neutral curve was constructed that relates the critical time and the disturbance wave number. It was found that the critical time also depends on the time at which the disturbance is introduced (unless this time is well before the smallest achievable onset time). More surprisingly, it also depends on the manner in which one attempts to define instability (i.e., on how one defines the strength of the evolving disturbance). The resulting neutral curves were compared with the results of a quasistatic or frozen-time approximate theory. The earliest onset time was the one that employed a thermal energy functional as the measure of the disturbance amplitude. In general, it was found that convection occurs much earlier than is predicted by the approximate theories. Moreover, and to one's initial surprise, it was found that growing cells always eventually restabilize and decay.

The linear theory was extended into the nonlinear regime in Part II in order to determine how finite-amplitude disturbances evolve. A mixed finite-difference and Fou-

rier series method was used to follow the evolution of nonlinear cells. Although detailed results were given on the effects of varying the initiation time and amplitude of the disturbance, the most important feature that was found is that even nonlinear cells eventually restabilize and decay. Indeed, nonlinear cells were found to restabilize earlier than their small-amplitude counterparts. This property of restabilization is seemingly at odds with the fact that the Darcy–Rayleigh number based on the thickness of the evolving basic state continues to grow, and therefore the whole configuration becomes increasingly thermoconvectively unstable with time. The aim of the present paper is to begin the process of resolving this apparent conflict.

In this paper, then, we are interested in the role played by secondary instabilities of the evolving nonlinear cells. That secondary instabilities should form the correct mode of disturbance may be predicted using the fact that the basic thermal boundary layer thickness grows in time, and larger wavelengths of cells (i.e., smaller wave numbers) are required to ensure that convection cells remain with roughly an $O(1)$ aspect ratio. The shape of the neutral stability curve is also such that the time interval over which growth can occur is much longer for smaller wave numbers. Therefore, it is worth investigating whether secondary disturbances with relatively small wave numbers can destabilize evolving nonlinear cells, thereby allowing strong convection to be maintained at later times.

We concentrate on the 2:1, 3:2, and 4:3 subharmonic cases where the respective wave numbers of the primary and subharmonic modes are in the ratio, m:n.

2. GOVERNING EQUATIONS AND BASIC SOLUTION

We are considering the instability of a basic state that is composed of a quiescent semi-infinite region of saturated porous medium at the uniform cold temperature T_∞, in which the lower horizontal boundary has its temperature raised suddenly to a new uniform level T_w, where $T_w > T_\infty$. The porous medium is considered to be homogeneous and isotropic, and the solid and fluid phases are in local thermal equilibrium. We assume that the flow is governed by Darcy's law modified by the presence of buoyancy and subject to the Boussinesq approximation. Thus, the governing equations for the fluid motion and temperature field for buoyancy-driven convection are expressed in the following nondimensional form:

$$\frac{\partial u}{\partial x} + \frac{\partial v}{\partial y} = 0 \tag{1a}$$

$$u = -\frac{\partial p}{\partial x} \tag{1b}$$

$$v = -\frac{\partial p}{\partial y} + \theta \tag{1c}$$

$$\frac{\partial \theta}{\partial t} + u\frac{\partial \theta}{\partial x} + v\frac{\partial \theta}{\partial y} = \frac{\partial^2 \theta}{\partial x^2} + \frac{\partial^2 \theta}{\partial y^2} \tag{1d}$$

The appropriate boundary conditions are as follows:

$$y=0: \ \ v=0, \ \ \theta=1 \quad \text{and} \quad y\to\infty: \ \ v,\theta\to 0 \tag{1e}$$

while $\theta = 0$ everywhere within the porous medium when $t = 0$. In Eqs. (1a) and (1b) x and y are the horizontal and vertical coordinates, respectively, while u and v are the corresponding seepage velocities. In addition, p is the pressure while θ is the temperature.

It is essential to mention that there is no physical length scale in this semi-infinite domain, but that it is possible to define a length scale in terms of the properties of the fluid and porous matrix:

$$L = \frac{\mu\alpha}{\rho g \beta K (T_w - T_\infty)} \tag{2}$$

where ρ, g, β, K, T_w, T_∞, μ and α are the reference density, gravity, coefficient of cubical expansion, permeability, wall temperature, ambient temperature, dynamic viscosity, and effective thermal diffusivity, respectively. This definition of the length scale means that the usual Darcy–Rayleigh number takes a unit value

$$\mathrm{Ra} = \rho g \beta K L (T_w - T_\infty)/\mu\alpha = 1. \tag{3}$$

After eliminating pressure p between Eqs. (1b) and (1c) and on introducing stream function ψ, which is defined according to

$$u = \frac{\partial \psi}{\partial y} \quad \text{and} \quad v = -\frac{\partial \psi}{\partial x} \tag{4}$$

then the continuity equation is satisfied. Equations (1b)–(1d) now reduce to the pair

$$\frac{\partial^2 \psi}{\partial x^2} + \frac{\partial^2 \psi}{\partial y^2} = \frac{\partial \theta}{\partial x} \tag{5a}$$

$$\frac{\partial \theta}{\partial t} + \frac{\partial \psi}{\partial x}\frac{\partial \theta}{\partial y} - \frac{\partial \psi}{\partial y}\frac{\partial \theta}{\partial x} = \frac{\partial^2 \theta}{\partial x^2} + \frac{\partial^2 \theta}{\partial y^2} \tag{5b}$$

which are to be solved subject to the boundary conditions

$$y=0: \ \ \psi=0, \ \ \theta=1 \quad \text{and} \quad y\to\infty: \ \ \psi,\theta\to 0 \tag{5c}$$

and the initial condition that

$$\psi = \theta = 0 \quad \text{at} \quad t = 0 \tag{5d}$$

Therefore, at $t = 0$, the temperature of the lower boundary of the semi-infinite region of porous medium is raised suddenly from 0 to 1 where it remains for all $t > 0$.

The basic conduction profile is independent of x with no flow, and the thermal energy equation reduces to

$$\frac{\partial \theta}{\partial t} = \frac{\partial^2 \theta}{\partial y^2} \tag{6}$$

Equation (6) admits the well-known solution,

$$\theta = \operatorname{erfc} \eta = \frac{2}{\sqrt{\pi}} \int_{\eta}^{\infty} e^{-\xi^2}\, d\xi \tag{7}$$

where the similarity variable is given by

$$\eta = \frac{y}{2\sqrt{t}} \tag{8}$$

In this paper we choose to consider disturbances to the basic profile given in Eq. (7) by transforming the governing equations into the new coordinate system (η, τ), where η is given above and $\tau = \sqrt{t}$; this transformation of t to τ avoids the explicit appearance of fractional powers of t within the governing equations. Equations (5a) and (5b) now become

$$4\tau^2 \frac{\partial^2 \psi}{\partial x^2} + \frac{\partial^2 \psi}{\partial \eta^2} = 4\tau^2 \frac{\partial \theta}{\partial x} \tag{9a}$$

$$2\tau \frac{\partial \theta}{\partial \tau} + 2\tau \left(\frac{\partial \psi}{\partial x} \frac{\partial \theta}{\partial \eta} - \frac{\partial \psi}{\partial \eta} \frac{\partial \theta}{\partial x} \right) = 4\tau^2 \frac{\partial^2 \theta}{\partial x^2} + \frac{\partial^2 \theta}{\partial \eta^2} + 2\eta \frac{\partial \theta}{\partial \eta} \tag{9b}$$

Given that the coefficient of θ on the right-hand side of Eq. (9a) increases with time, it is clear that the strength of the buoyancy forces also increases. Physically, the thickness of the region over which the temperature varies from 1 on the lower boundary to a nominal value, such as 0.01, also increases with time, and therefore a local Rayleigh number based on the thermal boundary layer thickness is seen to increase.

3. NUMERICAL METHOD

In Part II, we undertook a numerical investigation of the nonlinear evolution of spanwise periodic disturbances by taking a truncated spanwise Fourier expansion of the form

$$\psi(x, \eta, \tau) = \sum_{n=1}^{N} \psi_n(\eta, \tau) \sin nkx \tag{10a}$$

$$\theta(x, \eta, \tau) = \operatorname{erfc} \eta + \frac{1}{2}\theta_0(\eta, \tau) + \sum_{n=1}^{N} \theta_n(\eta, \tau) \cos nkx \tag{10b}$$

where k is the wave number and N is the truncation level. In Part I we retained only the ψ_1 and θ_1 terms since they were assumed to be infinitesimally small in magnitude. Therefore, nonlinearities were neglected in order to form a linearized stability theory. In Part II ψ_1 and θ_1 formed the primary mode and this mode interacted with itself to induce components with wave numbers $2k$, $3k$, and so on. The term $\frac{1}{2}\theta_0$ yields the mean change to the basic state due to the presence of convective cells. In this paper we shall refer to the pair (ψ_n, θ_n) as mode n.

The substitution of the expansions (10) into Eqs. (9a) and (9b) is very lengthy to present and has been omitted for the sake of brevity. The resulting system is comprised of $2N + 1$ second-order partial differential equations in η and τ. In the numerical simulations of Part II, the truncation level was chosen to be $N = 5$, which was sufficient since the magnitude of θ_5 was always very small compared with unity. The full system was then solved by a standard Keller-box method using the numerical differentiation methodology described by Lewis et al. (1997) to obtain the Newton–Raphson iteration matrix.

In the present paper we are interested in how subharmonic disturbances destabilize the solutions obtained in Part II. For the 2:1 subharmonic case, mode 2 (which has wave number $2k$) is termed the primary mode, while mode 1 is the potentially destabilizing subharmonic. For the 3:2 case, mode 3 forms the primary mode while mode 2 is the subharmonic disturbance. This naming scheme follows in the obvious way for the 4:3 subharmonic case.

In general, then, thermal disturbances are introduced at the initiation time $\tau = \tau_i$ for a given wave number k and the disturbance profiles take the form

$$\theta_n = A_n \eta e^{-3\eta} \tag{11}$$

where A_n is the amplitude of the mode n disturbance. Part II showed that the mode shape is largely irrelevant, as the disturbances quickly evolve to a common shape that is essentially independent of the initial disturbance shape and time of introduction. For the nonlinear study of Part II we set $A_1 = A$ and $A_n = 0$ otherwise. Here, for the 2:1 case, both A_1 and A_2 will be nonzero with $A_2 > A_1$, since mode 2 is to be destabilised by mode 1. All other A_n values will be set to zero. Likewise, for the 3:2 case

we will have $A_3 > A_2$ with all other values of A_n set to zero.

Given that $N = 5$ was the smallest truncation level that yielded reliable results in Part II, we need to take $N = 10$ for the 2:1 case, $N = 15$ for the 3:2 case, and $N = 20$ for the 4:3 case.

A rectangular domain in η and τ was used where η ranges from 0 to 10 with the uniform step of 0.05, this maximum value of η being sufficient to contain the evolving disturbance, while a step length of 0.1 was used in the τ direction.

For reference, Fig. 1 depicts the neutral stability characteristics obtained in Part I, and forms the context into which to set the present computations. Two neutral curves are shown, namely, that obtained using a quasistatic theory (continuous curve) and that obtained by using an energy integral to determine the magnitude of the evolving disturbance (symbols). Disturbances decay when the wave number and time correspond to locations below the curve, to the right of the right-hand branch and to the left of the left-hand branch, otherwise they grow. For the quasistatic approximate theory disturbances for which $k > 0.101053$ (see Part I) are always destined to decay, i.e., they are stable. All other disturbances decay until they first cross the curve vertically, after which point they grow, but then they restabilize and decay upon crossing the upper branch of the curve. The equivalent maximum wave number for the exact theory is $k = 0.1124$.

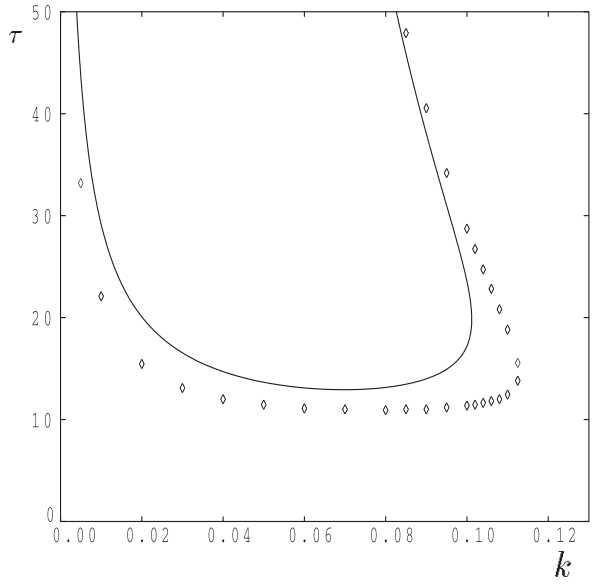

FIG. 1: Neutral stability curve: τ against k.

Of more importance is the earliest time after which disturbances grow; for the quasistatic theory this critical time and its associated wave number are given by

$$\tau_c = 12.944356 \quad \text{and} \quad k_c = 0.069623 \tag{12a}$$

while the corresponding data for the exact theory are

$$\tau_c = 8.9018 \quad \text{and} \quad k_c = 0.07807 \tag{12b}$$

Thus, disturbances always decay when $\tau < 8.9018$.

4. NUMERICAL RESULTS

In this section we present a detailed account of how the presence of subharmonic disturbances affects the evolution of the primary mode. In all cases we shall take $\tau_i = 8$ as the initiation time for both the primary and the subharmonic. This leaves us with a choice of the wave number, the type of subharmonic (i.e., 2:1, 3:2, or 4:3), and the amplitudes of the initiating disturbances. The strength of the various horizontal Fourier modes may be gauged in terms of the surface rate of heat transfer of each:

$$q_n(\tau) = \left.\frac{\partial \theta_n}{\partial \eta}\right|_{\eta=0} \tag{13}$$

The overall evolution of the flow is also assisted by the heat transfer footprint of disturbance, $q(x, \tau)$, which is defined as follows:

$$q(x, \tau) = \frac{1}{2} q_0 + \sum_{n=1}^{N} q_n(\tau) \cos nkx \tag{14}$$

The expression for q is useful, in particular, for showing how many convection cells are present at any point in time, and for showing when the peak rates of heat transfer occur.

4.1 The 2:1 Subharmonic Case

In this case we specify a relatively large value of amplitude A_2 of mode 2 (the primary mode) and attempt to destabilize it with a small disturbance in the form of mode 1. Figure 2 represents a typical set of cases where the wave number of the subharmonic is $k = 0.035$, so that the primary mode has a wave number of 0.07. We have chosen $A_2 = 10^{-1}$ as the initial amplitude of the primary mode. A selection of values of A_1 have been used to show the influence of the amplitude of the subharmonic on how quickly the primary mode is destabilized. Also included is the basic case with $A_1 = 0$ in order to show how the

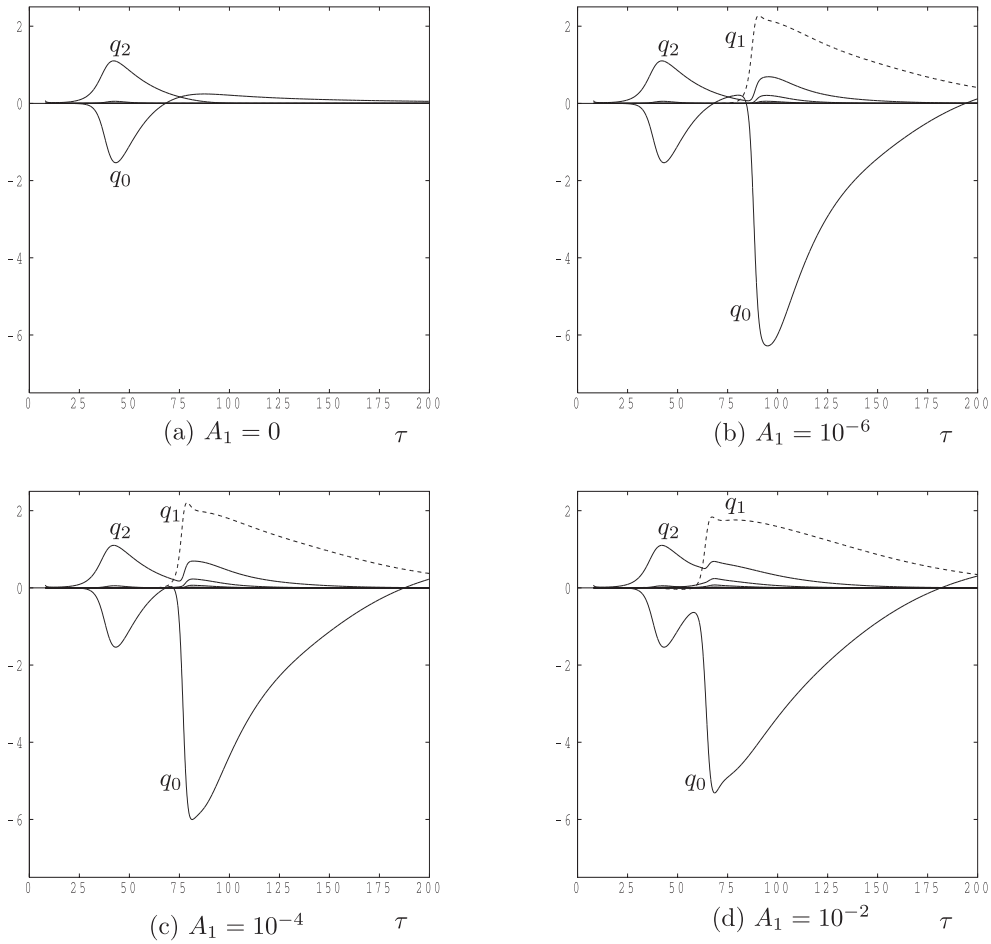

FIG. 2: Variation with τ of the surface rates of heat transfer, q_n, corresponding to the modes, $n = 0, 1, 2 \cdots$. These simulations correspond to $\tau_i = 8$, $k = 0.035$, and $A_2 = 10^{-1}$ and a selection of values of A_1.

primary mode varies without subharmonic disturbances being present. Solutions are presented in terms of the surface rate of heat transfer of the different Fourier modes.

Concentrating first on the unrestricted evolution of the primary mode, for which $A_1 = 0$, both Fig. 2 and the data it represents show that the primary mode begins to grows at a time that is roughly consistent with the $k = 0.07$ mode in Fig. 1. It is worthy of note that the neutral curve shown in Fig. 1 corresponds to a thermal energy criterion which gives an earlier onset time a curve which is based on the surface rate of heat of heat transfer; see Part I for a detailed discussion of this point. The primary mode then decays at $\tau \equiv 45$, which is well before the stabilization time for linear theory, which is roughly $\tau \equiv 75$. The strength of the nonlinear convection may be gauged by the magnitude of $\frac{1}{2}q_0$, which, at its peak, almost doubles the rate of heat transfer due to the basic temperature profile. Therefore, strongly nonlinear effects have altered the x-independent background state from that of the solution given in Eq. (7), and it is this that causes the premature restabilization when compared with linearized theory.

Concentrating now on how subharmonic disturbances alter the evolution of the primary mode, Fig. 2 also presents the effect of three different subharmonic amplitudes, $A_1 = 10^{-6}$, 10^{-4}, and 10^{-2}, while keeping all other parameters fixed. We note that the subharmonic, for which $k = 0.035$, has a later onset time and a much later restabilization time than the primary mode, which has a wave number of 0.070, at least for linearized theory (see Fig. 1). In all three cases the subharmonic appears very suddenly while the primary mode is undergoing a slow decline. In fact, when A_1 is much smaller than 10^{-2}, the primary

mode has already decayed substantially before the subharmonic begins to grow, and the late appearance of the subharmonic is due entirely to how small its amplitude has become since $\tau = \tau_i$ and the need to be able to grow again to an $O(1)$ magnitude. However, when A_1 is as large as 10^{-2}, the subharmonic grows well before the primary modes decay greatly. Figure 2 also shows that destabilization of the primary mode occurs increasingly early as A_1 increases, but that the peak magnitude of q_0 decreases as A_1 increases. In Figs. 1 and 2 the behavior of the higher modes is most easily illustrated by noting the heights of the various maxima situated at $\tau \simeq 90$ in Fig. 2(b); here, the highest maximum corresponds to mode 1, the next to mode 2, and so on.

The behavior of the mean rate of heat transfer q_0 also deserves some discussion. In Part II we saw that the maximum magnitude of q_0 is attained at roughly the same time as the maximum value of the heat transfer since the primary mode is attained. The large value of q_0 is a consequence of the fact that the mean temperature field has been altered substantially by the strongly nonlinear convection pattern. Thereafter, the magnitude of q_0 decreases rapidly, and q_0 itself changes sign. This feature also occurs here. However, when the primary mode is destabilized, the magnitude of q_0 rises rapidly once more as the subharmonic mode is established, and then it falls away again as the subharmonic mode eventually begins to decay.

Figure 3 shows an alternative view of the solutions shown in Fig. 2 by depicting the isolines of the surface rate of heat transfer of the disturbance as a function of x and τ; i.e., the heat transfer footprint given by Eq. (14). In each subfigure, contours are drawn using 20 equally spaced intervals centered at zero. Therefore, the levels vary from subfigure to subfigure. Four whole wavelengths of the primary mode are depicted, but the subharmonic instability reduces this to two wavelengths. The evolution of the primary mode, for which $A_1 = 0$, shows a clear period of growth followed by decay. The strength of the nonlinearity is indicated by the lack of symmetry between neighboring thermal cells. The four strongest cells correspond to situations where the fluid is moving toward the surface, bringing cold fluid downward and increasing the rate of heat transfer. The weaker cells, which interleave the stronger ones, correspond to outflow, and these rise up from the surface (see Part II).

When subharmonic disturbances are present, the initial evolution of the primary mode is unaffected until well after they have achieved their maximum rate of heat transfer. In fact, the bottom half of each of the subfigures with $A_1 \neq 0$ are almost identical to the subfigure with $A_1 = 0$. However, once the subharmonic appears, the primary cells are destroyed rapidly, as seen by the very close spacing of the isotherms. In fact, the subharmonic is so strong that the alternate cells have lifted from the surface, as will be seen in Fig. 4(a). Thus, the contours in the very top parts of the nonzero A_1 subfigures correspond to two periods. Figure 3 also shows very clearly how different values of A_1 affect the time at which the subharmonic appears.

Figures 4(a) and 4(b) show the detailed isotherms and streamlines of the evolving disturbance, respectively, at various values of τ for the $A_1 = 10^{-2}$ case, which is covered in Figs. 2 and 3. In Figs. 2 and 3, two whole horizontal periods of the primary mode are depicted, and this corresponds to one period of the subharmonic. In Fig. 4(a),

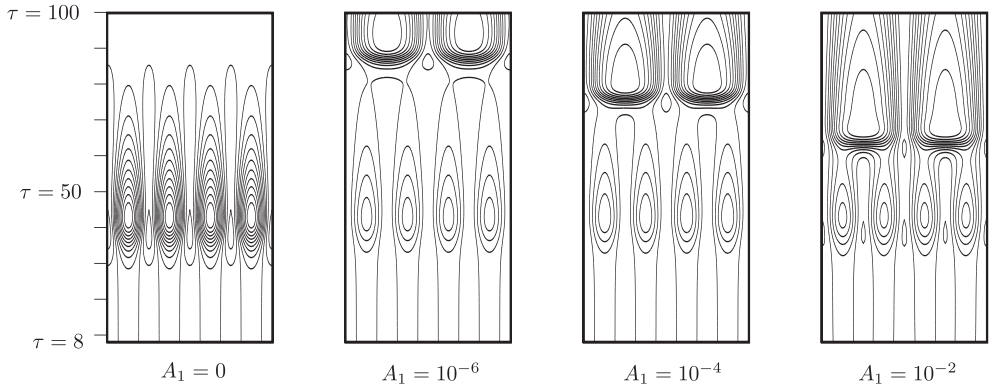

FIG. 3: Isolines of the surface rate of heat transfer, $q(x, \tau)$, for the wave number, $k = 0.035$, using $\tau_i = 8$, $A_2 = 10^{-1}$, and a selection of values of A_1. The horizontal coordinate varies between $x = 0$ and $x = 8\pi/k$; i.e., four horizontal periods, and the vertical axis varies between $\tau = \tau_i = 8$ and $\tau = 100$.

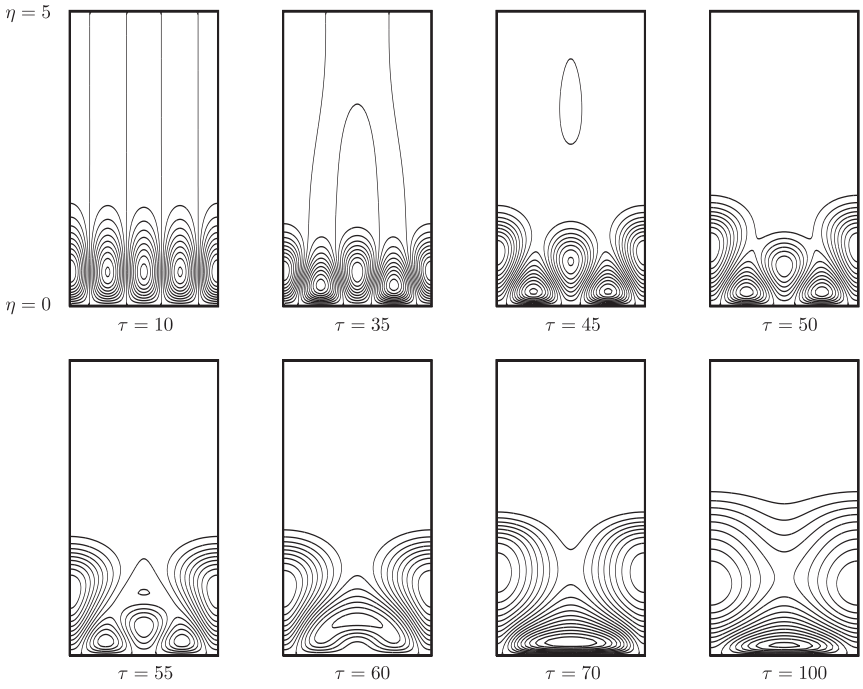

(a)

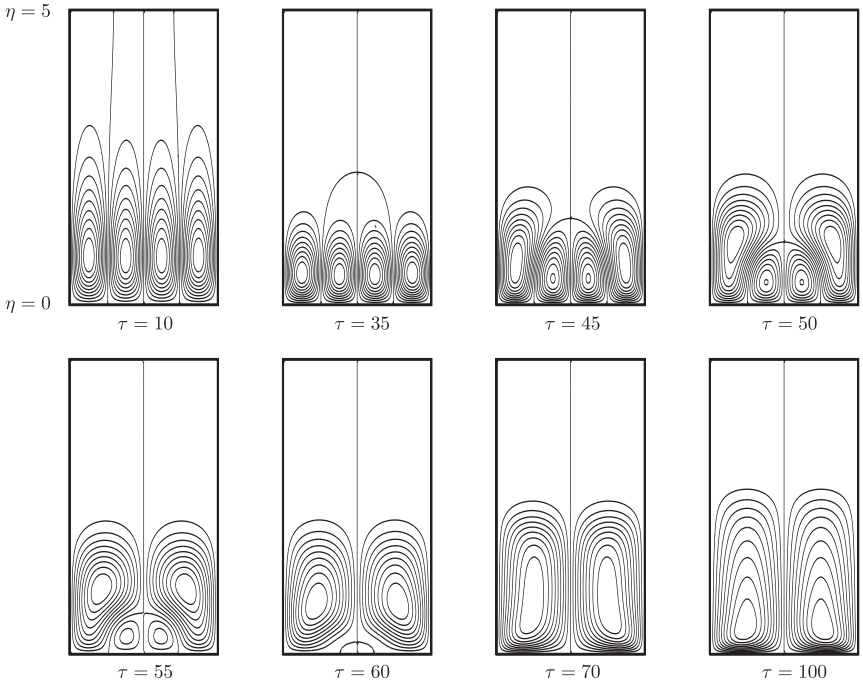

(b)

FIG. 4: (a) Contours of the perturbation temperature profiles and **(b)** streamlines of the flow at chosen times for the evolution of the subharmonic instability given by $\tau_i = 8$, $k = 0.035$, $A_1 = 10^{-2}$, and $A_2 = 10^{-1}$. The horizontal coordinate varies between $x = 0$ and $x = 4\pi/k$; i.e., two horizontal periods.

the transition from the fully developed primary mode to the fully developed subharmonic is shown. At first, the two thermal cells on either side of the central cell shrink compared with the others due to inflow, and it is these cells which are responsible for the higher rates of heat transfer seen in Fig. 3. When $\tau = 50$, the outer half-cells have grown to such an extent that all three cells in the middle are smaller. Although the central cell was larger than its two nearest neighbors when $\tau = 35$, it shrinks and does so to such an extent that these neighbors drive it to extinction at the surface, whereupon they grow and merge. At $t = 70$ the process is complete and the rate of heat transfer at the heated surface is now very large indeed, as is seen by the closeness of the isotherms there, and by the magnitude of q_0 in Fig. 2. When $\tau = 100$ the isotherm spacing has increased, thereby reducing the surface rate of heat transfer once more.

Figure 4(b) depicts the corresponding behavior of the streamlines and this shows an alternative view of the subharmonic instability. Between $\tau = 10$ and $\tau = 35$ the momentum boundary layer decreases in thickness. This happens because each ψ_n function, as given in Eq. (9a), satisfies an equation of the form

$$\psi_n'' - 4n^2k^2\tau^2\psi_n = -4nk^2\tau^2\theta_n \qquad (15)$$

and therefore, for a given k, the e-folding distance decreases as τ increases. After $\tau = 35$ the inner two cells gradually weaken forming a pair of recirculating regions which gradually diminish in size and strength. Just after $\tau = 60$ they disappear, leaving a relatively thick region where the subharmonic forms the dominant solution. The e-folding distance of the subharmonic is double that of the primary mode, which is why the disturbance has roughly doubled in thickness. At later times the thickness of the subharmonic will begin to decrease once more.

Figure 5 shows a summary of the situation depicted in Figs. 2–4 and of a much larger set of computations. Figure 5 displays what we shall call the transition time as a function of the initial amplitudes of the primary mode and the subharmonic. The transition time τ_s is defined as being that time at which the values of q_1 and q_2 have exactly the same magnitude. The value a on the abscissa corresponds to an initial subharmonic amplitude of $A_1 = 10^{-a}$ (i.e., $a = -\log_{10} A_1$), while the different symbols correspond to different initial primary cell amplitudes; these are indicated in the caption to Fig. 5.

The interpretation of Fig. 5 is as follows. Below the horizontal line all modes of the chosen wave number decay, but the primary mode begins to grow upon crossing the line, as the line represents the onset criterion. Given the information represented by Fig. 2, the primary mode then reaches a maximum and subsequently decays. When the symbol representing the chosen value of A_2 is encountered, it is at this point in time that the surface heat transfer due to the growing subharmonic q_1 is equal to that of the decaying primary mode, as given by q_2.

Focusing first on the case $k = 0.04$, for which the primary mode has a wave number of 0.08, it is clear that for a chosen value of A_2, the transition time increases with increasing value of a, i.e., for decreasing amplitudes of the subharmonic disturbance. This happens because it takes a longer time for the subharmonic to grow until it reaches an $O(1)$ magnitude. When we consider the variation in the transition time as a function of A_2, it is also clear that the transition time increases as A_2 decreases. This behavior may be understood easily, for a reduction in the strength of the primary mode requires a less strong subharmonic to destabilize it.

When $k = 0.035$ we obtain a similar pattern of transition times as for $k = 0.04$, but they occur later because the primary mode has the wave number 0.07, which is very close to the critical wave number given in Eq. (12), and therefore it grows more strongly than that given in Fig. 5(a). This trend continues as k is reduced, and becomes more marked because the linearized onset time for the subharmonic now begins to grow quite rapidly compared with that for the primary mode. Thus, the 2:1 subharmonic route to destabilization becomes less effective for these wave numbers.

A corollary of the above conclusion is that if the primary mode is sufficiently weak, then the subharmonic may even be too strong for the "primary" mode to become established. In fact, the absence of data below $\tau \simeq 32$ in Fig. 5(a) is because the subharmonic grows in preference to the primary mode and establishes itself first. This also explains the presence of some "anomolous" transition points in Fig. 5(d) for smaller values of a; in this case, the data points represent a reverse transition where the mode with the smaller wave number is destabilized by the mode with the higher wave number.

When the wave number of the primary mode is greater than 0.08 (and the subharmonic has a wave number greater than $k = 0.04$), the opposite effect is true. In this case, the transition times are earlier because the onset times for the primary mode and its subharmonic are much closer, as may be seen in Fig. 1, and there is now only a small interval of time over which the primary mode can grow. Therefore, this primary mode is easier to destabilize using subharmonic disturbances.

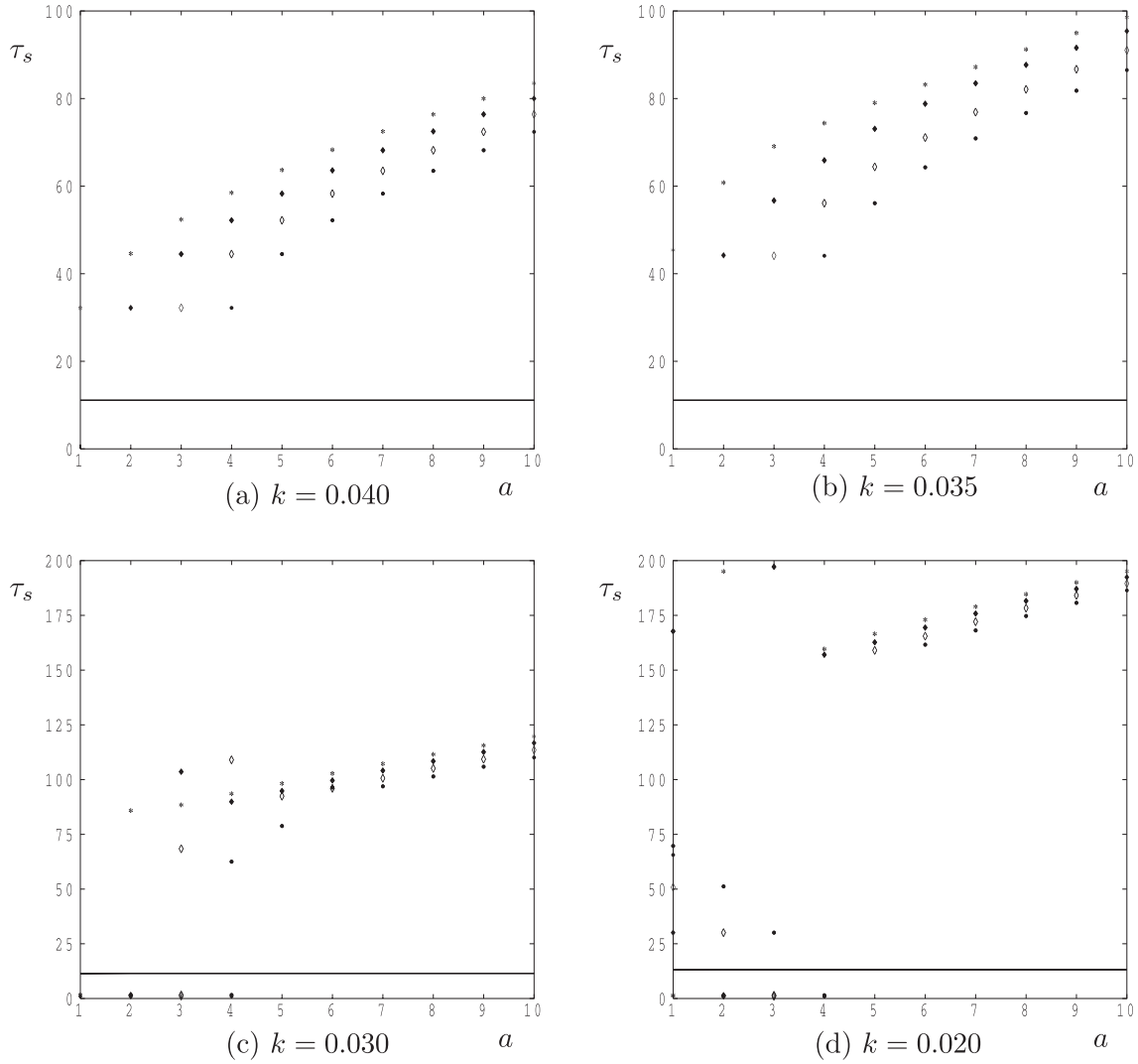

FIG. 5: Variation in the values of the transition time, τ_s, with $a = -\log_{10} A_1$ for different values of A_2 for the wave numbers **(a)** 0.04, **(b)** 0.035, **(c)** 0.03, and **(d)** 0.02. The line near to $\tau = 13$ corresponds the onset of instability of the primary cell. The symbols •, ◊, ♦, and $*$ refer to $A_2 = 10^{-1}$, 10^{-2}, 10^{-3}, and 10^{-4}, respectively.

4.2 The 3:2 Subharmonic Case

We now turn to the 3:2 subharmonic route to destabilization. Here, we consider the primary mode to have wave number $3k$ while the disturbance has wave number $2k$. We shall consider two cases in detail, namely, those for which the primary mode has wave numbers 0.07 and 0.09. These cases represent the typical behavior found during our various simulations.

We consider first the case where $3k = 0.07$. We take $A_3 = 0.1$ as the disturbance amplitude of the primary mode, $A_1 = 0$, and A_2 taking the values, 0, 10^{-6}, 10^{-4}, and 10^{-2}. Figure 6 represents the variation of the surface rate of heat transfer q_n with τ.

When $A_2 = 0$, both q_3, the surface rate of heat transfer of the primary mode, and q_0, the mean change of heat transfer, follow precisely the same evolutionary path as shown in Fig. 2 when neglecting the influence of the subharmonic disturbance, as the wave number of the primary mode is the same in both cases. The other three subfigures show how the primary mode is affected by the presence of three different subharmonic disturbances. In all three

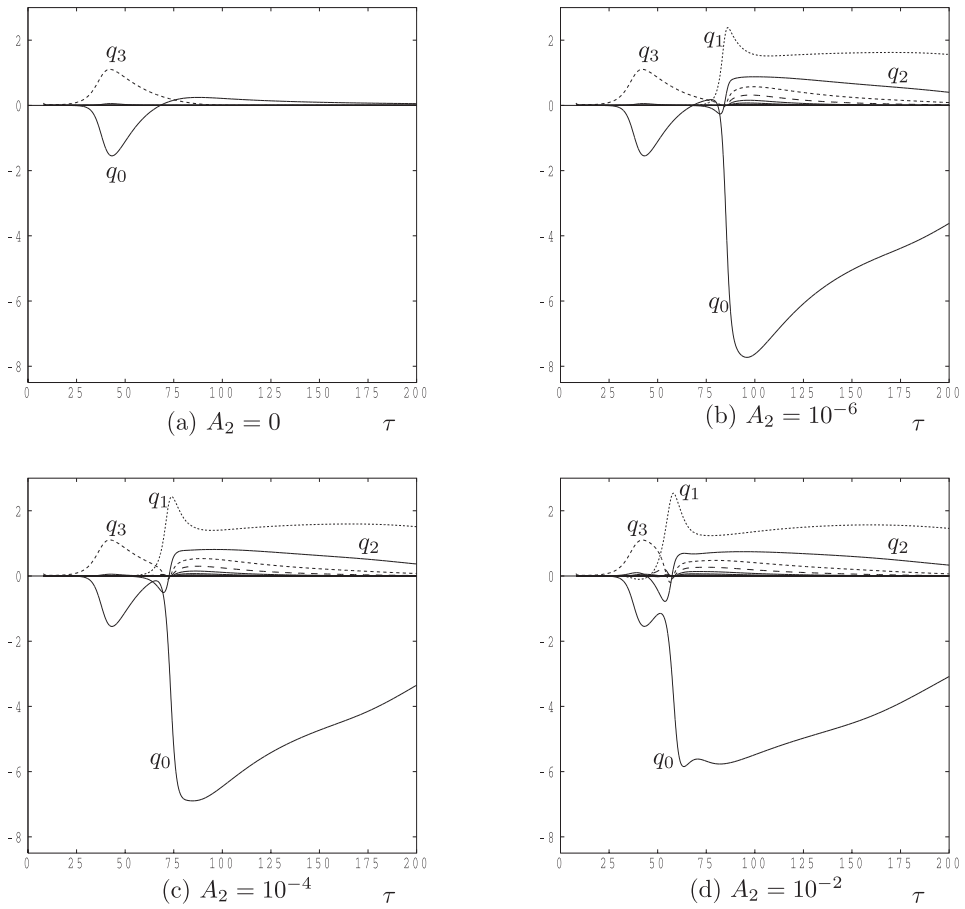

FIG. 6: Variation with τ of the surface rate of heat transfer, q_n, corresponding to the modes, $n = 0$, 1, 2, and 3. The simulations correspond to $\tau_i = 8$, $3k = 0.07$, and $A_1 = 0$; $A_3 = 10^{-1}$; and a selection of values of A_2. Short dashes: q_1; medium dashes: q_3; long dashes: q_4; unbroken curves: q_0, q_2, and all other modes—this convention also applies to Figs. 9 and 12.

of these cases, q_1 and q_2 begin to grow at roughly the same rate, although with different signs. However, mode 1 eventually grows faster, takes over as the dominant mode, with mode 2 following the growth of mode 1 as the latter is the first superharmonic of the former.

On comparing Fig. 6 with Fig. 2, we see that mode 1 also grows very rapidly here, although it is not the subharmonic mode that was introduced. Of interest is the fact that destabilization occurs earlier for the 3:2 case than for the 2:1 case, and the largest absolute mean change to the surface heat transfer q_0 achieves larger values. Thus, it would appear that the 3:2 destabilization is stronger in its effect than the 2:1 case.

Isolines of the surface rate of heat transfer of disturbances $q(x, \tau)$ are shown in Fig. 7 for the cases displayed in Fig. 6. As before, contours are drawn using 20 equally spaced intervals in each subfigure with the middle contour corresponding to a zero value of q. The growth and decay of the primary mode, i.e., when $A_2 = 0$, is shown for reference. The chief difference between these isolines and those in Fig. 3 is that the peak rate of heat transfer for the present case is maintained at a roughly constant level after mode 1 has become established, whereas, for the 2:1 case, the heat transfer begins to decay steadily just after the peak is reached. In fact, this feature is more evident when comparing the q_1 curves in Fig. 6 with those in Fig. 3.

Figures 8(a) and 8(b) represent the detailed isotherms and streamlines of the evolving disturbance, respectively, at different chosen times for the $A_2 = 10^{-2}$ case. Three

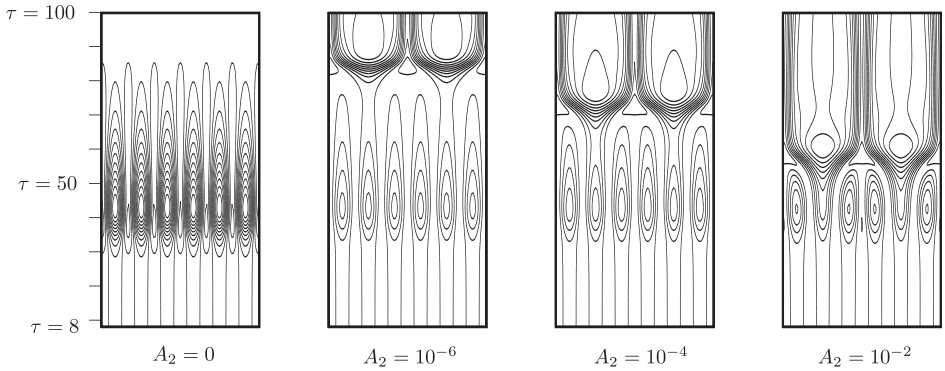

FIG. 7: Isolines of the surface rate of heat transfer, $q(x, \tau)$, for $3k = 0.07$, using $\tau_i = 8$, $A_1 = 0$, $A_3 = 10^{-1}$, and a selection of values of A_2. The horizontal coordinate varies between $x = 0$ and $x = 12\pi/k$; i.e., six horizontal periods, and the vertical axis varies between $\tau = \tau_i = 8$ and $\tau = 100$.

periods of the primary mode are shown and these reduce to one period of mode 1. The evolution of the thermal cells with time is fairly complex and centers around the fact that next-but-one neighbors are not equal in strength. Nonlinear competition then serves to inhibit some thermal cells and to enhance others. If, in the top row of Fig. 8(a), we were to label the cells from 0 to 6, then cells 0 and 2 combine first, thereby eliminating cell 1. The same happens between cells 4 and 6 where cell 5 is eliminated. In the meantime, the middle cell grows and we are left with just one period of a cellular pattern. During the transition, then, two cells disappear while two pairs merge; therefore, at no time do we see a pattern which is at all like a mode 2 pattern with two periods being evident. A similar process happens with the streamlines in Fig. 8(b). Both sets of figures yield a rapidly expanding region of activity, one that is much larger than is depicted in Fig. 4, and this is because the e-folding distance according to Eq. (15) is larger due to k being smaller here than for the cases shown in Fig. 4.

Essentially the same figures are now reproduced in Figs. 9–11 for the case where the primary mode has a wave number of 0.09. We show these because qualitatively different behavior may be found for this choice of wave number.

Figure 1 shows that the expected interval of growth of a mode with a wave number of 0.09 is relatively short, although significant growth can happen. The $A_2 = 0$ subfigure of Fig. 9 appears to show little activity, but this is simply scaled in the same way as for the remaining subfigures. On the other hand, the $A_2 = 0$ subframe of Fig. 10 shows clearly the period of time over which growth occurs, and the mismatch between neighboring thermal cells shows that the mode has become nonlinear, although not strongly so.

Figure 9(b), for which $A_2 = 10^{-6}$, gives an evolutionary behavior that is identical qualitatively to those shown in Fig. 6, in that while mode 2 destabilizes the primary mode (mode 3), it is mode 1 that appears. On the other hand, when the initial amplitude of mode 2 is increased to $A_2 = 10^{-4}$, there is a clear, but short, interval in which mode 2 is dominant before it, too, is overtaken by mode 1. This may be seen in Fig. 10(c) at the point marked by an asterisk where there are now four periods showing, as compared with the original six periods. At larger values of τ there are only two periods of the mode 1 cell.

However, when $A_2 = 10^{-2}$, the successive transitions from mode 3 to mode 2 and from mode 2 to mode 1 takes place in a very clear way with long intervals of time during which each mode is dominant. Interestingly, Fig. 9(d) shows that the transition from mode 2 to mode 1 yields a negative value of q_1, which means that this final transition, a 2:1 subharmonic in effect, yields a pattern that is 180° out of phase with those shown in Fig. 3. Figure 10(d) gives an exceptionally clear representation of both transitions.

Some instantaneous isotherms and streamlines of the evolving disturbance corresponding to the previous two figures are shown in Figs. 11(a) and 11(b) for the cases $A_1 = 0$, $A_2 = 10^{-2}$, and $A_3 = 10^{-1}$. In Figs. 11(a) and 11(b) we see that six cells at $\tau = 10$ transform into four cells at $\tau = 50$ by cell merging and removal, and then into two cells at $\tau = 100$. Of particular interest is the very rapid evolution between $\tau = 90$ and $\tau = 100$, where the cells that are placed close to the heated surface strengthen suddenly.

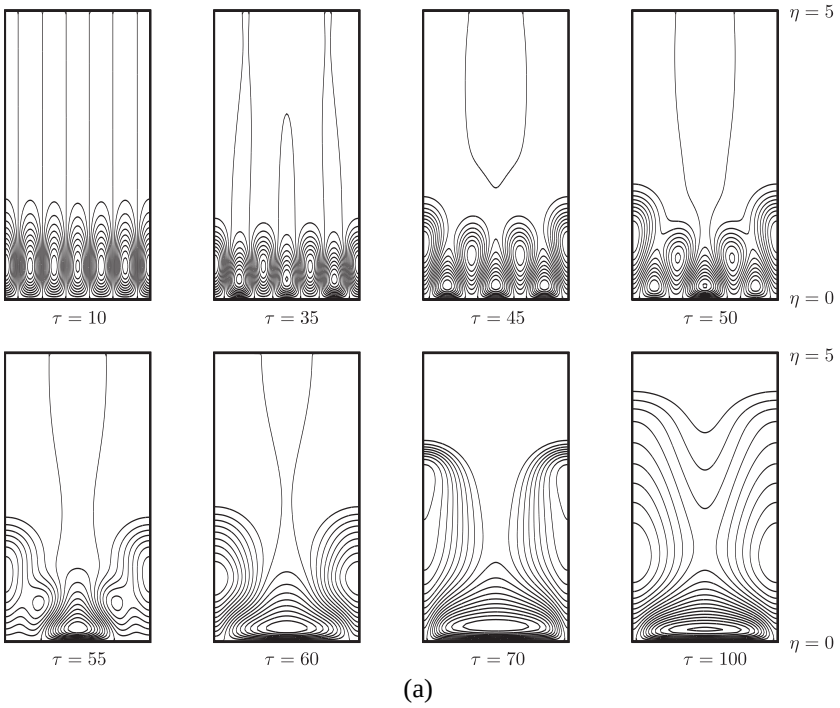

(a)

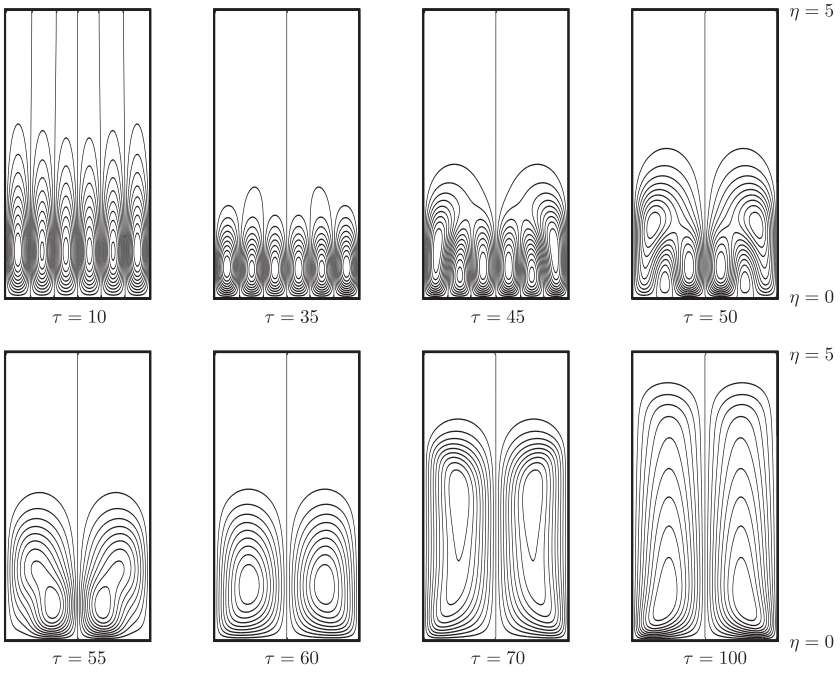

(b)

FIG. 8: (a) Contours of the perturbation temperature profiles, and **(b)** streamlines of the evolving flow, at chosen times for the evolution of the subharmonic instability given by $\tau_i = 8$, $3k = 0.07$, $A_1 = 0$, $A_2 = 10^{-2}$, and $A_3 = 10^{-1}$. The horizontal coordinate varies between $x = 0$ and $x = 6\pi/k$; i.e., three horizontal periods.

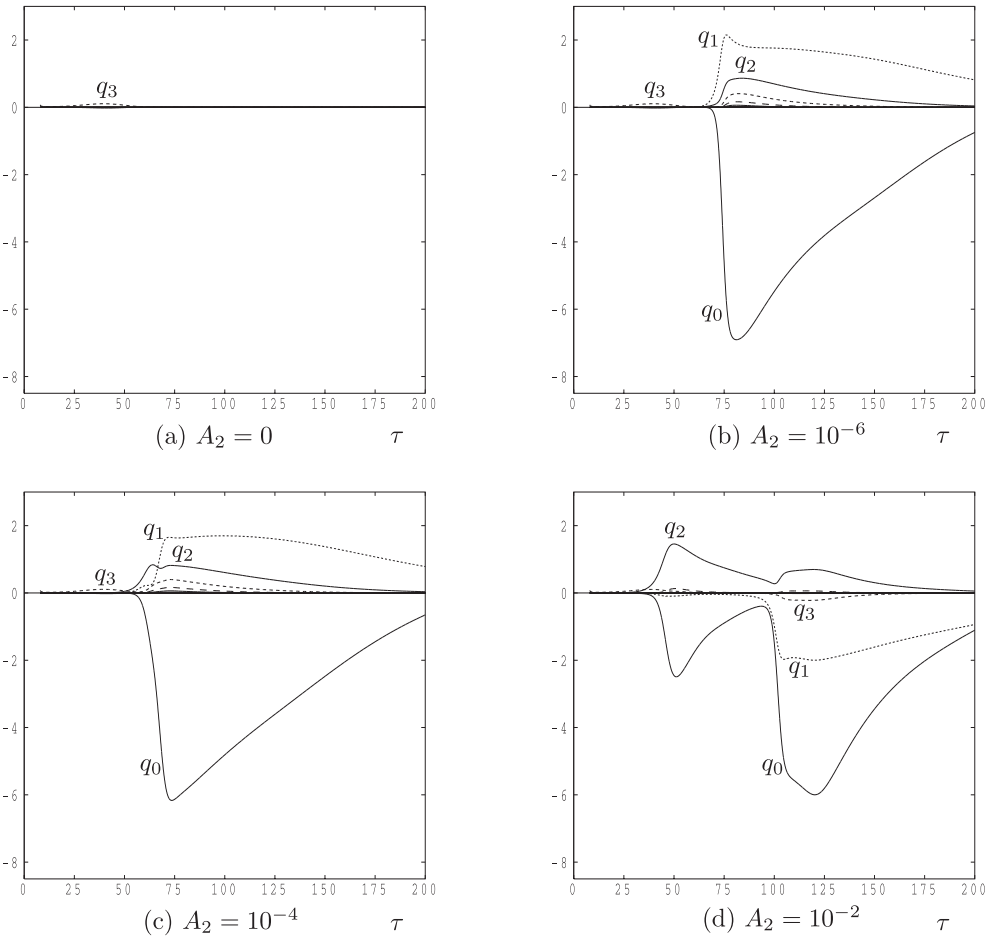

FIG. 9: Variation with τ of the surface rate of heat transfer, q_n, corresponding to the modes, $n = 0$, 1, 2, and 3. The simulations correspond to $\tau_i = 8$, $3k = 0.09$ and $A_1 = 0$, $A_3 = 10^{-1}$, and a selection of values of A_2.

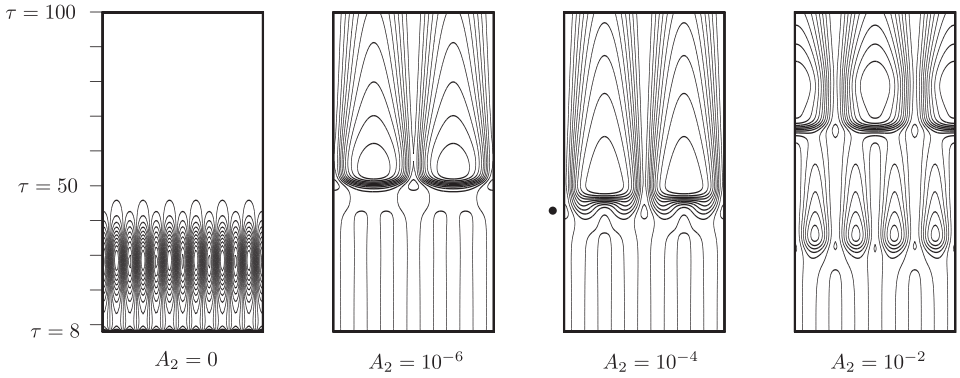

FIG. 10: Isolines of the surface rate of heat transfer, $q(x, \tau)$, for the wave number, $3k = 0.09$, using $\tau_i = 8$, $A_1 = 0$, $A_3 = 10^{-1}$, and a selection of values of A_2. The horizontal coordinate varies between $x = 0$ and $x = 12\pi/k$; i.e., six horizontal periods, and the vertical axis varies between $\tau = \tau_i = 8$ and $\tau = 100$.

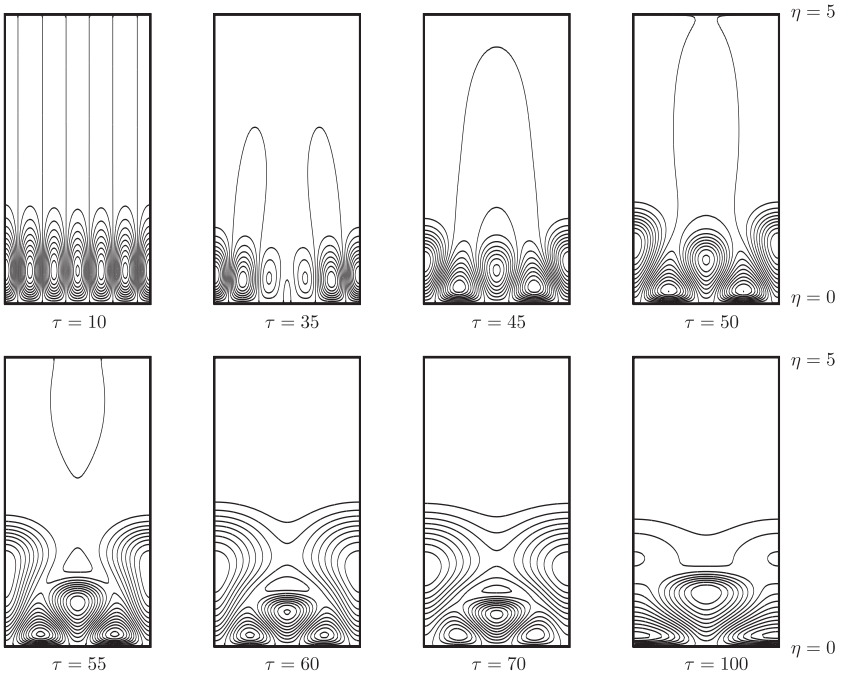

(a)

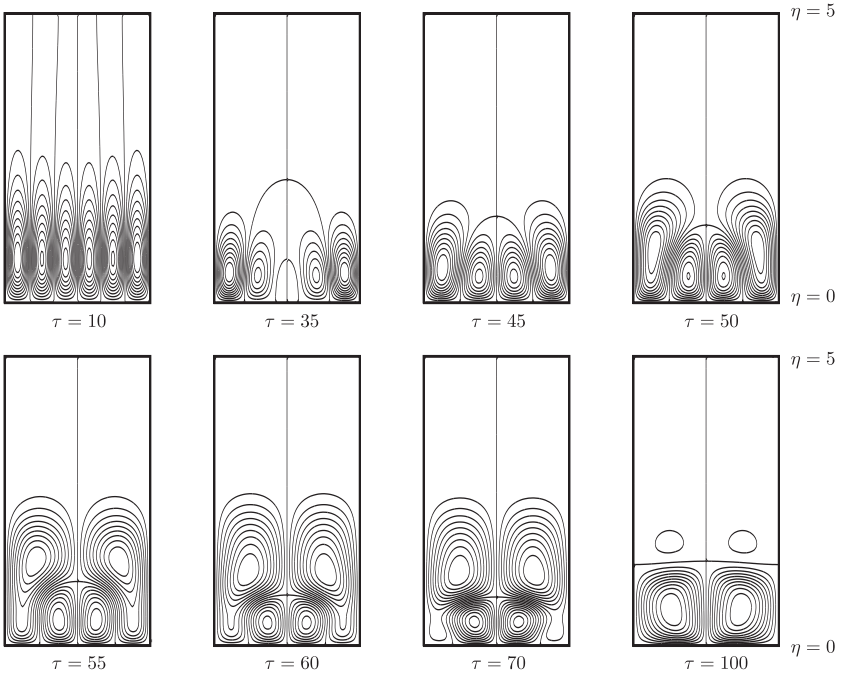

(b)

FIG. 11: (a) Contours of the perturbation temperature profiles, and **(b)** streamlines of the evolving flow, at chosen times for the evolution of the subharmonic instability given by $\tau_i = 8$, $3k = 0.09$, $A_1 = 0$, $A_2 = 10^{-2}$, and $A_3 = 10^{-1}$. The horizontal coordinate varies between $x = 0$ and $x = 6\pi/k$; i.e., three horizontal periods.

4.3 The 4:3 Subharmonic Case

Now we will concentrate on the 4:3 subharmonic case, where modes 3 and 4 in the Fourier expansion represent the subharmonic and primary modes, respectively.

Figure 12 represents the variation of the surface rate of heat transfer q_n with τ. The wave number of the primary mode is given by $4k = 0.07$, and therefore the subharmonic has wave number $3k = 0.0525$. The initial amplitudes of modes 1 and 2 are set to zero, and for the primary disturbance we take $A_4 = 10^{-1}$. As above, we have used the following amplitudes for subharmonic disturbance: $A_3 = 0$, 10^{-6}, 10^{-4}, and 10^{-2}, where $A_3 = 0$ is equivalent to having no subharmonic disturbance. We note that we have again chosen the primary mode to have wave number 0.07, so that all three subharmonic cases (namely, 2:1, 3:2, and 4:3) may be compared.

Figure 12 shows the evolution of the various q_n values with τ, and we find that the ultimate fate of flow depends on the magnitude of the subharmonic disturbance. When $A_3 = 10^{-6}$ the primary mode has decayed almost to nothing before mode 2 makes a brief appearance prior to the establishment of mode 1 as the dominant mode. When A_3 takes larger values, the modal exchanges that take place favor mode 2 as the final convecting state, at least for $\tau \leq 200$. We suspect that mode 1 will destabilize the evolving mode 2 pattern at later times, although we have not tested this hypothesis.

Of interest is the fact that the mean change to the surface rate of heat transfer q_0 is substantially larger when $A_3 = 10^{-6}$ than when A_3 takes the two larger values depicted in Fig. 12. Thus, the magnitude of the response is not necessarily in proportion to the magnitude of the disturbance, but depends on complicated modal exchanges.

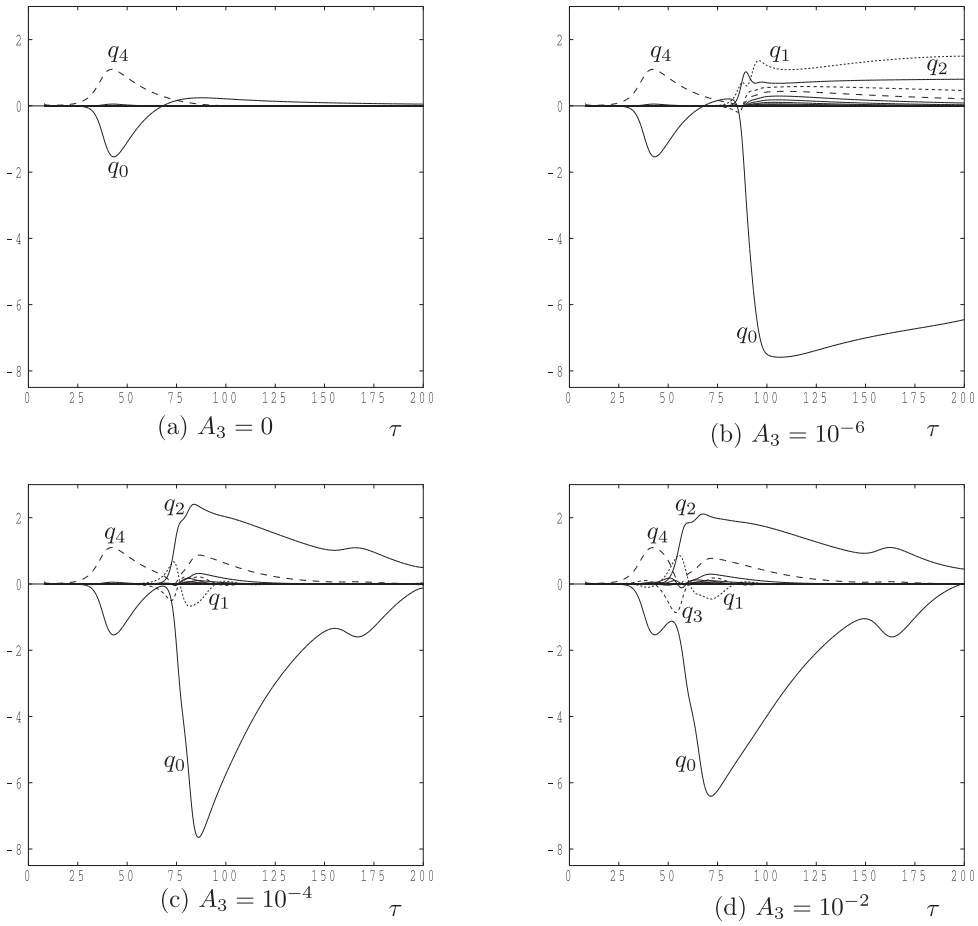

FIG. 12: Variation with τ of the surface rate of heat transfer, q_n, corresponding to the modes, $n = 0$, 1, 2, and 3. The simulations correspond to $\tau_i = 8$, $4k = 0.07$ and $A_1 = 0$, $A_2 = 0$, $A_4 = 10^{-1}$, and a selection of values of A_3.

The surface rates of heat transfer corresponding to the four subfigures in Fig. 12 are depicted in Fig. 13. Here, we see that the initial destabilization of the primary mode is indeed later for the smaller disturbance amplitudes, as one might expect intuitively.

Figure 14 shows instantaneous isotherms and streamlines for the $A_3 = 10^{-2}$ case, for which mode 2 emerges as the dominant mode. We have chosen this case particularly because the surface heat transfer data shown in Fig. 13 do not give a full picture of the complicated evolution that takes place. Concentrating first on the isotherms shown in Fig. 14(a), by the time $\tau = 45$, the thermal cells have either risen or fallen depending on whether they are located where there is outflow or inflow. Moreover, the amount by which the rising cells have risen varies and the pattern is reminiscent of the Eckhaus (or sideband) instability, which is a well-known destabilization mechanism for Bénard–like problems. When $\tau = 55$, the disturbance pattern has modified rapidly into a form that looks superficially like a mode 1 pattern. However, the central cell of this pattern has a detailed three-cell structure close to the surface, and it is this structure that causes q_2 to dominate in Figs. 12 and 13, and that grows strongly as τ increases further. In fact, when $\tau = 100$ the disturbance pattern is a rather unusual mixture of mode 2 near the heated surface and mode 1 further away.

Similar comments may be made about the evolution of the streamlines in Fig. 14(b). The Eckhaus amplitude modulation is very clear when $\tau = 10$, and so is the dual modal structure when $\tau = 100$.

5. DISCUSSION AND CONCLUSIONS

In this paper we have investigated various types of subharmonic instability of an evolving cellular pattern in an unsteady thermal boundary layer in a porous medium. This is an extension of the nonlinear simulations presented in Part II where it was found that, contrary to expectations, the nonlinearly developing cells are always eventually restabilized. In the present paper we have paid particular attention to the 2:1, 3:2, and 4:3 subharmonic cases, and these have all been found to destabilize the primary mode of convection. For the 2:1 case we have provided a comprehensive set of information on how the transition time between the primary and the subharmonic depends on the initial amplitudes of each disturbance. For the 3:2 case we have found two different routes to destabilization: one where mode 3 evolves directly into mode 1 and the other where there is a double transition with mode 3 giving way to mode 2 and then to mode 1. We have also shown some simulations for the 4:3 case, where we have obtained an unusual pattern that consists of one mode near the heated surface and another further away. We have also found that the strength of the response to subharmonic disturbance (in terms of the change in mean rate of heat transfer) is not a smooth function of the amplitude of the disturbance because the identity of the dominant mode also depends on that amplitude.

Given that the passage of time may be interpreted as an increasing Darcy–Rayleigh number, Ra, it is worth making some comparisons with the classical Darcy–Bénard

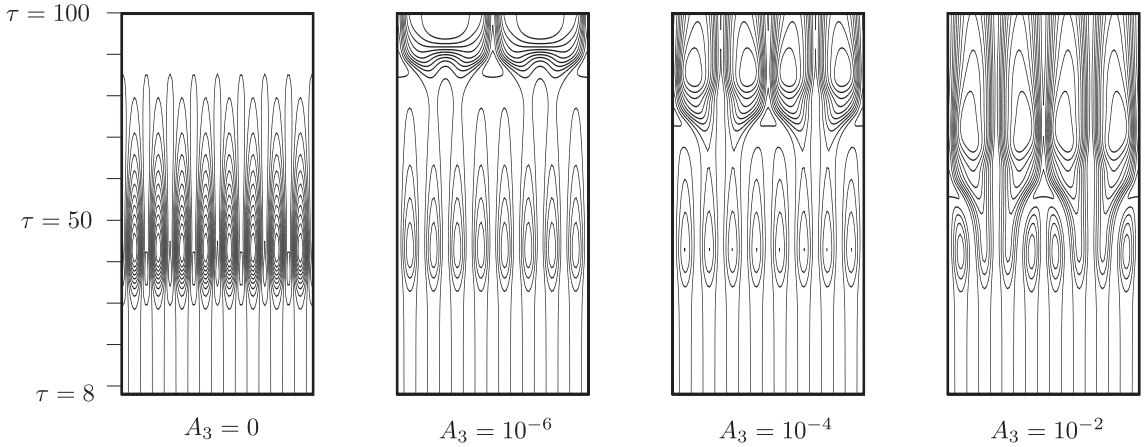

FIG. 13: Isolines of the surface rate of heat transfer, $q(x, \tau)$, for the wave number, $4k = 0.07$, using $\tau_i = 8$, $A_1 = 0$, $A_2 = 0$, $A_4 = 10^{-1}$, and a selection of values of A_3. The horizontal coordinate varies between $x = 0$ and $x = 16\pi/k$; i.e., eight horizontal periods, and the vertical axis varies between $\tau = \tau_i = 8$ and $\tau = 100$.

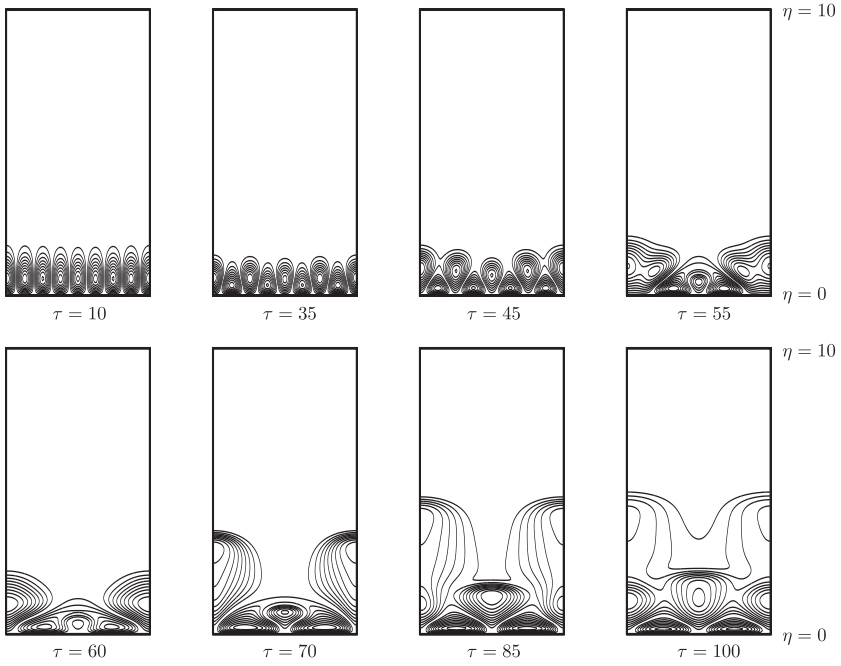

(a)

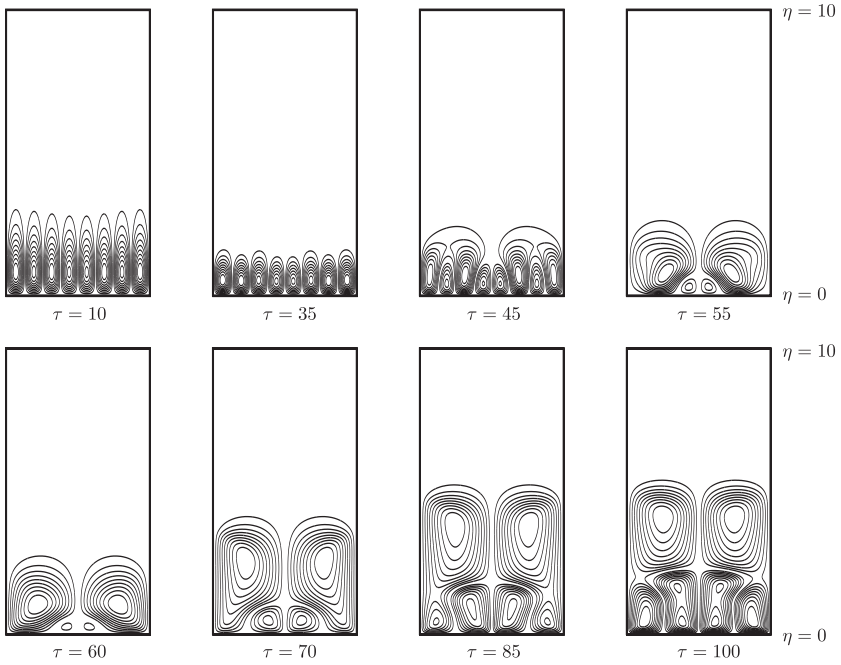

(b)

FIG. 14: (a) Contours of the perturbation temperature profiles, and **(b)** streamlines of the evolving flow, at chosen times for the evolution of the subharmonic instability given by $\tau = \tau_i = 8$, $4k = 0.07$, $A_1 = A_2 = 0$, $A_3 = 10^{-2}$, and $A_4 = 10^{-1}$. The horizontal coordinate varies between $x = 0$ and $x = 8\pi/k$; i.e., four horizontal periods.

problem. The first comprehensive study of the stability of large-amplitude convection in a uniform layer heated from below was undertaken by Straus (1974), who determined the region in wave number/Ra space in which steady two-dimensional convection is stable. Generally, as Ra increases, the range of wave numbers for which convection is stable moves toward higher wave numbers. This is consistent with the computations of Georgiadis and Catton (1986), who found the wave number that corresponds to the largest rate of heat transfer at any chosen value of Ra also increases as Ra increases. The implication of the shape of the stability envelope of Straus (1974) is as follows: should Ra be increased slowly or quasistatically, then eventually convection at the chosen (and originally stable) wave number becomes unstable, and the primary instability mechanism is a cross-roll disturbance with a larger wave number. This observation marks a major qualitative difference between the Darcy–Bénard problem and the present unsteady thermal boundary layer where destabilization causes a reduction in the observed wave number. Although our present calculations are confined to two dimensions, we would expect that any three-dimensional instability mechanism would also consist of roll disturbances (within the linear regime, at least), whose wave number is smaller than that of the evolving pattern; this is the implication of the previously mentioned tendency of cells to try to maintain a roughly $O(1)$ aspect ratio as the boundary layer thickens in time.

Our numerical simulations have the nature of a highly controlled experiment. The adoption of the Fourier ansatz in Eq. (10) means that the results are not affected by noise, taking the form of small-scale random fluctuations, such as one would have quite naturally in a porous medium. In addition, we have not considered the effect of isolated disturbances, nor of three-dimensionality. Indeed, the fact that most of Straus's (1974) stability envelope corresponds to the cross-roll instability suggests that three-dimensional effects may also be significant here. It is also quite certain that the various transitions that we have observed will change should the initiation time we have adopted be changed. In addition, the cascade of instabilities that our computations suggest as a possible destabilization mechanism cannot continue to much later times because the detailed numerical studies of Kimura et al. (1986) and Riley and Winters (1991) suggest that the narrow thermal boundary layer which occurs in the convection cells near to $\eta = 0$ (see the $\tau = 100$ frames in Figs. 4 and 8, for example) may itself be destabilized by traveling waves, thereby leading to yet another potential destabilization mechanism in the present context.

We certainly intend to investigate how isolated disturbances propagate, and preliminary work seems to suggest that the convection cells that are induced tend to have a wavelength that increases with time (Selim 2009). Riaz et al. (2006) also provides much information on chaotic cellular development in two dimensions, but as yet no three-dimensional simulations have been undertaken; it is hoped that this issue also will be addressed in the near future.

ACKNOWLEDGEMENTS

The first author would like to thank the University of Bath for a Departmental Studentship and an Overseas Research Award to enable this research to be undertaken. The authors would like to thank the reviewers for their excellent comments which have served to improve the quality of the manuscript.

REFERENCES

Carslaw, H. S. and Jaeger, J. C., *Conduction of heat in solids*, Oxford University Press, Oxford, 1986.

Ennis-King, J. P. and Paterson, L., Role of convective mixing in the long-term storage of carbon dioxide in deep saline formations, *SPE J.*, vol. **10**, no. 3, pp. 349–356, 2005.

Georgiadis, J. G. and Catton, I., Prandtl number effect on Bénard convection in porous media, *ASME J. Heat Transfer*, vol. **108**, pp. 284–290, 1986.

Kimura, S., Schubert, G., and Straus, J. M., Route to chaos in porous-medium convection, *J. Fluid Mech.*, vol. 166, pp. 305–324, 1986.

Lewis, S., Rees, D. A. S., and Bassom, A. P., High wavenumber convection in tall porous containers heated from below, *Q. J. Mech. Appl. Math.*, vol. **50**, pp. 545–563, 1997.

Rees, D. A. S., Selim, A., and Ennis-King, J. P., The Instability of Unsteady Boundary Layers in Porous Media, *Emerging topics in heat and mass transfer in porous media—from bioengineering and microelectronics to nanotechnology*, (Peter Vadasz, ed.), Springer, pp. 85–110, 2008.

Riley, D. S. and Winters, K. H., Time-periodic convection in porous media: The evolution of Hopf bifurcations with aspect ratio, *J. Fluid Mech.*, vol. **223**, pp. 457–474, 1991.

Riaz, A., Hesse, M., Tchelepi, H. A., and Orr, F. M., Onset of convection in a gravitationally unstable diffusive boundary layer in porous media, *J. Fluid Mech.*, vol. **548**, pp. 87–111, 2006.

Selim, A., Instability of unsteady boundary layers in porous media, Ph.D. thesis (University of Bath), 2009.

Selim, A. and Rees, D. A. S., The instability of a developing

thermal front in a porous medium. I Linear theory, *J. Porous Media*, vol. **10**, pp. 1–15, 2007a [Part I].

Selim, A. and Rees, D. A. S., The instability of a developing thermal front in a porous medium. II Nonlinear evolution, *J. Porous Media*, vol. **10**, pp. 17–33, 2007b [Part II].

Socolow, R. H., Can we bury global warming?, *Sci. Am.*, July, pp. 49–55, 2005.

Straus, J. M., Large amplitude convection in porous media, *J. Fluid Mech.*, vol. **64**, pp. 51–63, 1974.

Wooding, R. A., Tyler, S. W., and White, I., Convection in groundwater below an evaporating salt lake. I. Onset of instability, *Water Resour. Res.*, vol. **33**, pp. 1199–1218, 1997.

Xu, T., Apps, J. A., and Pruess, K., Numerical simulation of CO_2 disposal by mineral trapping in deep aquifers, *Appl. Geochem.*, vol. **19**, pp. 917–936, 2004.